Electrosynthesized copper polycorroles as versatile materials in double lateral heterojunctions

Lorena Di Zazzo, Abhishek Kumar, Rita Meunier-Prest, Corrado Di Natale, Roberto Paolesse, Marcel Bouvet

Graphical abstract

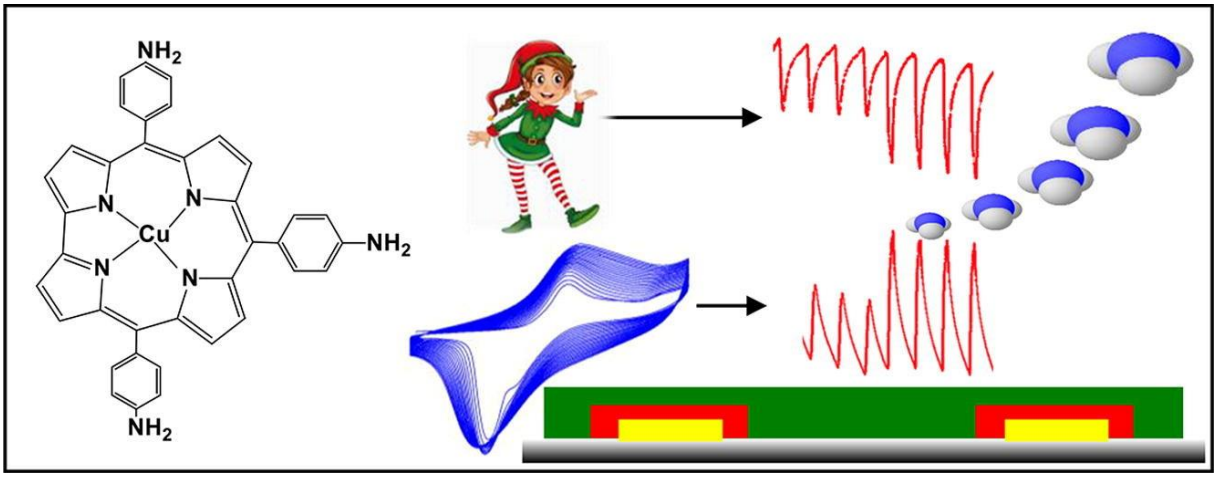

- First copper corrole polymers have been synthesized
- Polycorroles have been implemented in organic electronic devices
- Depending on deposition conditions, devices exhibit p- or n-type behavior
- Impedance spectroscopy shows the key role played by interfaces
- The sensors operate at RT with a sub-ppm LOD (125 ppb)

Electrosynthesized copper polycorroles as versatile materials in double lateral heterojunctions

Lorena Di Zazzo[1,2], Abhishek Kumar[1], Rita Meunier-Prest[1], Corrado Di Natale[2]*, Roberto Paolesse[3]*, Marcel Bouvet[1]*

[1] Institut de Chimie Moléculaire de l'Université de Bourgogne (ICMUB), UMR CNRS 6302, Université Bourgogne Franche-Comté, 9 avenue Alain Savary, 21078 Dijon cedex, France. Fax: +33-380-396-098; Tel: +33-380-396-086; E-mail: marcel.bouvet@u-bourgogne.fr

[2] Department of Electronic Engineering, University of Rome Tor Vergata, Via Politecnico 1, 00133 Roma, Italy

[3] Department of Chemical Science and Technology, University of Rome Tor Vergata, Via della Ricerca Scientifica, 00133, Roma

*Corresponding authors: dinatale@uniroma2.it (C. D. M.), roberto.paolesse@uniroma2.it (R. P.), marcel.bouvet@u-bourgogne.fr (M. B.)

Abstract

Metallocorrole derivatives are an emerging class of coordination complexes successfully exploited in different applications, ranging from catalysis to medical field, due to their peculiar tunable properties. Herein, new polycorroles materials are *in situ* synthesized and deposited on the electrodes in a one-step electrochemical method from 5,10,15-(4-aminophenyl)corrolato]copper(III) as monomer, generating phenazine bridges containing polymer chains. Conductive films are obtained and the film thickness can be controlled by tuning the number of potential scans. However, the nature of the resulting polymer is affected by the electropolymerization conditions: in neat CH_2Cl_2 the protonation of polymer chains occurs. The role of proton scavenger 2,6-lutidine is worth mentioning, which prevents demetallation of corrole macrocycle. The polycorrole films are further combined with lutetium bis-phthalocyanine to realize double lateral heterojunction (DLH) sensors for ammonia detection, in which organic-organic interface plays a key role in their charge transport properties. The protonation of polycorrole can tune the p- or n-nature of the semiconducting film, and the highest sensitivity obtained with these devices favorably competes with these reported so far for DLH heterojunctions, with a limit of detection as low as 125 ppb for NH_3.

Introduction

Among molecular materials used in organic electronics, metallomacrocycles have drawn wide interests, owing to their optoelectronics properties tailoring by molecular engineering [1-5]. Beyond the single macrocycle unit, phthalocyanine (MPc) and porphyrin (MP) polymers were also reported [6,7]. Polyphthalocyanines can be obtained directly starting from 1,2,4,5-tetracyanobenzene [6], while different routes have been reported for the preparation of polymeric porphyrins. A first approach exploits the direct link of macrocycles by oxidation of meso-free diaryl porphyrins; depending on the strength of oxidizing species, *meso-meso* coupling or *meso-meso* and β–β couplings can occur using mild and strong oxidants, respectively, forming one or three C-C bonds [8,9], leading, in the latter case, to the formation of the so-called "porphyrin tapes" [10]. Another route is to electropolymerize porphyrins bearing electroactive substituents [11]. In this case, electrochemical oxidation can result into generation of the two types of polymers, depending on the application of mild or high anodic potential [12-14]. A typical example is the electrochemical oxidation of tetrakis-(4-aminophenyl)porphyrins, forming C-N bonds and in some conditions to phenazine bridged porphyrins (Fig. 1) [15,16]. In the last few years, additionally to phthalocyanine and porphyrin macrocycles a different tetrapyrrole, the corrole (Fig. 1), has attracted the attention of researchers, because of some interesting peculiarities of its chemistry [17,18]. Corrole is a contracted porphyrin, with a molecular skeleton featuring that of corrin, the nucleus of Vitamin B12. Corrole was reported for the first time in the early 60s [19], as a by-product of the rush for the definition of the synthetic route to Vitamin B12. It gained renewed attention recently, after the discovery of simple synthetic routes for its preparation [20,21], because both its coordination chemistry and its photophysical properties led to some initial promising applications [22], going from catalysis [23] to the medical field for fighting cancer [24].

In particular, corrole complexes have shown interesting performances as electrocatalysts for oxygen reduction reaction (ORR) [25,26], a process of paramount importance for energy conversion. During these studies it was shown that polycorroles, obtained by electropolymerization of tris(p-aminophenyl) cobalt (III) corrole [27] and 5,15-bis(p-aminophenyl),10-pentafluorophenyl cobalt (III) corrole [26] were more efficient as ORR catalysts than the monomers, in terms of reaction mechanism and kinetics. Although these examples demonstrated the peculiar and promising properties of corrole derivatives, the

exploitation of corroles in the field of chemical sensors is still in infancy, and only sparse reports are present for the preparation of poly-corroles [28]. Some of us demonstrated the application of corroles as sensing materials in chemical sensors and have successfully exploited them as functional layers in Quartz crystal microbalances (QCM) and optical sensors [22]. Thus, QCM sensors based on octamethyl derivative of manganese corrole was combined with metalloporphyrins into an electronic nose (e-nose) setup to identify biomarkers of lung cancer in the breath analysis [29]. Other corrole derivatives were reported as sensing layers to detect range of volatile organic compounds, CO and NO vapors, with QCM [30] or surface acoustic wave (SAW) tranducers [31]. Despite some recent reports of corroles application in gas sensors, the application of these materials in emerging sensing methods, such as organic heterojunction sensors, is missing, which have demonstrated promising application in NH_3 detection at room temperature [32]. Organic heterojunction sensors comprise an organic heterostructure as a sensing layer, formed by combining different organic semiconductors in diverse configurations. These sensors benefit from the high interfacial charge transport at the organic-organic junction, owing to the accumulation of mobile charges [33], which impart high metrological performances to the respective sensors [34,35].

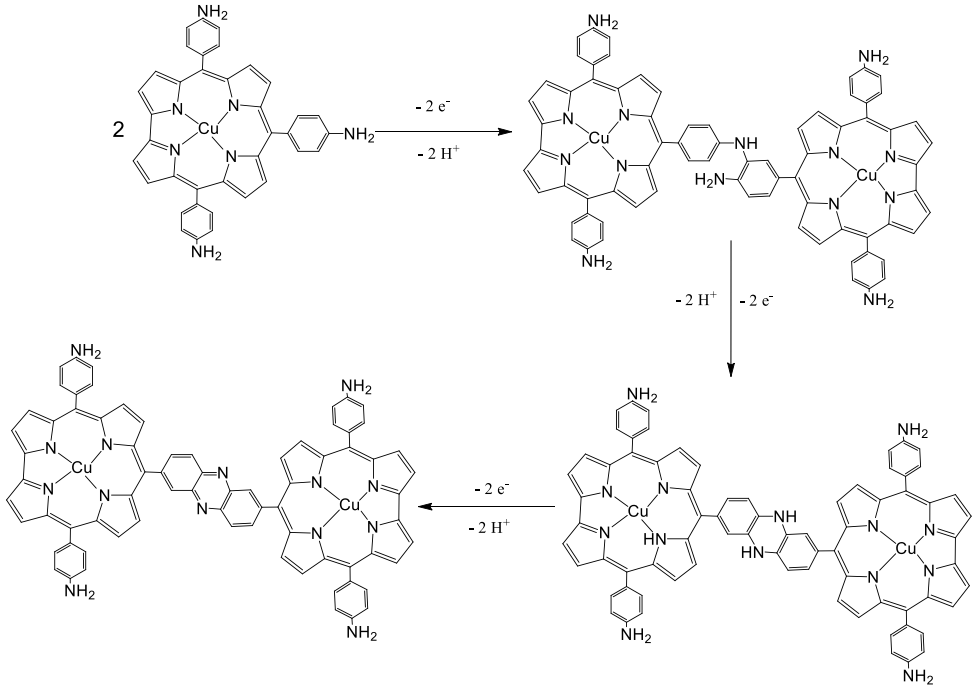

Figure 1. Mechanism of polymer formation through phenazine bridges, starting from 5,10,15-(4-aminophenyl)corrolato]copper(III), CuTpNH_2PC (top left).

Among different organic semiconductors, metal porphyrinoids have found significant applications in organic heterojunction sensors [32, 36]. Some configurations of organic heterojunction sensor use a low conducting sublayer and a high conducting top layer, such that the former strongly influence the interfacial charge transport, while the latter interacts with the gas molecules. In such sensors, lutetium bis-phthalocyanine ($LuPc_2$) was used in most of the cases as top layer, owing to its high intrinsic carrier density and electronic conductivity [2,37]. On the other hand, different types of low conducting materials have been used as sublayer to modulate the charge transport process and thus to improve the gas sensing performances [38-42]. Although, multitudes of previous literature report heterojunction sensors based on MPc and MP, metallocorroles or their polymers have not been yet studied in such sensors. However, corroles can be highly promising, owing to their structural similarity with MPc and MP, which can be engineered to impart different electronic properties. Moreover, such materials are highly electrochemically active and are compatible with different electrical transducers. In the present heterojunctions, the sub-layer does not interact directly with the target gas but determines the transport properties of the device. Thus, polycorroles can be suitable to develop organic heterojunction sensors for NH_3 detection, which monitoring in widely sought in food industries and agricultural activities. A limit of detection (LOD) in the ppm range is require for many applications [43], as in food industries (e.g. 30-200 ppm in cheese ripening cellars) and a sub-ppm LOD for applications in the field of breath analysis (tens of ppb for healthy people with increase in case of liver or kidney malfunctioning, up to ca. 1 ppm) [44,45].

In this endeavor, in the present work, we report the first synthesis of copper polycorroles and their integration into organic heterojunction sensor for NH_3 detection by combining with $LuPc_2$, which is a well-known intrinsic semiconductor [2,37,46]. The key novel feature from the material aspect is that new polycorrole materials are *in situ* synthesized and coated on the sensor electrodes in one-step electropolymerization reactions by using 5,10,15-(4-aminophenyl)corrolato]copper(III) ($CuTpNH_2PC$) as a precursor. Thin film of the new polycorroles materials have been characterized by optical spectroscopies, cyclic voltammetry and X-ray photoelectron spectroscopy (XPS) to evaluate their electroactivity, electronic properties and structural features. The electrical behavior and nature of interfaces in polycorrole/$LuPc_2$ heterojunction devices are studied through current-voltage and impedance spectroscopy measurements. Different heterojunction sensors are then exposed towards

ammonia vapor, NH_3, in a wide concentration and relative humidity (RH) ranges and various metrological parameters have been determined. Finally, the interaction of NH_3 on the sensor surface is modelled based on Langmuir adsorption isotherm.

Experimental methods

Reagent and chemicals

General procedure for the synthesis of [5,10,15-(4-aminophenyl)corrolato]copper(III) ($CuTpNH_2PC$): 50 mg of $CuTpNO_2PC$ (0.069 mmol) were dissolved in 25 ml of CH_2Cl_2/CH_3OH 4:1 v/v. 5 mg of Pd/C and 114 mg of $NaBH_4$ (2.77 mmol) were added, stirring the solution under reflux for 45 minutes. The solution, after the addition of $NaBH_4$, initially changed color to green and after 30 minutes turned to brown. The progress of the reaction was monitored via TLC (silica gel and CH_2Cl_2/CH_3OH as eluent system) and UV-Vis spectroscopy. After the disappearance of starting material, the reaction mixture was filtered on a celite plug to remove the catalyst and then the solvent was evaporated. The crude was taken up in CH_2Cl_2 and purified with a silica gel chromatographic column using CH_3OH 2% v/v in $CHCl_3$ as eluent system. The main product identified as $CuTpNH_2PC$ was crystallized in CH_2Cl_2/petroleum ether (1:2 v/v) as brown crystals with a yield of 52% (22.7 mg) [47].

^1H NMR (300 MHz, $CDCl_3$): 7.90 – 7.89 (d, 2H, β-pyrroles), 7.80 – 7.78 (d, 2H, βpyrroles), 7.71 – 7.68 (d, 4H, phenyls), 7.63 – 7.60 (d, 2H, phenyls), 7.45 (s, 4H βpyrroles), 6.83 – 6.77 (m, 5H, phenyls), 3.95 (s, 6H, NH). MS (FAB): m/z 632 (M+).

Lutetium bisphthalocyanine ($LuPc_2$) was synthesized according to the literature [48]. Dichloromethane was procured from a local supplier and was distilled before use in solutions preparation. 2,6-Lutidine (2,6-dimethylpyridine; 99%), tetrabutylammonium perchlorate (> 98%) (TBAP), potassium chloride (KCl) and potassium hexacyanoferrate ($K_3[Fe(CN)_6]$) were purchased from Sigma-Aldrich.

Electrochemical setup and electropolymerization of $CuTpNH_2PC$

ITO coated glass plate (9 mm diameter of active surface, 8-12 Ω of square resistance, Solems, France) and IDE of ITO (interdigitated electrodes deposited onto 1 x 1 cm^2 float glass substrate and separated by 75 µm with 50 nm thickness) were cleaned for 10 min each in dichloromethane, acetone, ethanol and distilled water for 10 min in the sonicator for three

times and dried under synthetic air flow. Teflon cell was washed in a solution of H_2SO_4/H_2O_2 3:1 v/v mixture and rinsed in distilled water. Electrochemical experiments were performed at PGSTAT302N Autolab Metrohm potentiostat interfaced with Nova 2.1 software. Cyclic voltammetry was carried out on a three-electrode setup consisting of an ITO plate or an IDE as working electrode, a platinum wire as a counter electrode, and a saturated calomel electrode (SCE) isolated from the solution by a salt bridge containing the same electrolyte solution as in cell to prevent any leakage of KCl into the cell. The electropolymerization of $CuTpNH_2PC$ was performed in the monomer solution (10^{-3} M) in CH_2Cl_2 + 0.1 M TBAP without or with lutidine (2,6-lutidine/CH_2Cl_2 5/95% v/v). The polymerization was carried out in a Teflon cell using a total volume of 400 µL, in potentiodynamic conditions by cyclic voltammetry (CV) in the range 0.1 to 0.8 V at a scan rate of 100 $mV.s^{-1}$. The CVs are recorded for 20 and 100 cycles to control the quantity of deposits on the electrode surface. After the polymerization, the electrodeposited films were rinsed with CH_2Cl_2 to remove the electrolyte and the unreacted monomer particles followed by drying in the ambient conditions. A similar procedure was repeated to deposit polymer films on ITO covered glass plate for the characterization studies. The polymer coated electrodes were studied by recording CV in 10^{-3} M $K_3[Fe(CN)_6]$ in 0.1 M KCl aqueous medium in the range of -0.2 to 0.8 V at a scan rate of 100 $mV.s^{-1}$.

Polymer film characterization

The UV-Vis spectra of the polymers coated on ITO plate were recorded on a Varian's Cary® 50 spectrophotometer, using Xenon flash lamp as an excitation source in the range of 300-900 nm. The spectrum of $CuTpNH_2PC$ solution was also recorded in the same range using a 10 mm quartz cuvette. Raman spectra of the polymers and $CuTpNH_2PC$ powder were acquired by using a Renishaw inVia Raman microscope using a 473 nm laser as an excitation source. The elemental and chemical analyses of the electropolymerized films on ITO were carried out by XPS using Versaprobe 5000 spectrometer (UMVAC-PHI apparatus), utilizing a monochromatic and focused Al Kα X-ray source (1486.6 eV). For each polymeric film on ITO, a survey spectrum and a high resolution core level spectrum of carbon 1s, nitrogen 1 s, oxygen 1 s and copper 2p were recorded over a 200 µm spot size. The pass energies were 187.5 eV and 58.7 eV for the survey and core-level spectra, respectively.

Development of device and ammonia sensing

The device is developed in a two-step process. Firstly, the polycorrole film is electropolymerized on ITO interdigitated electrodes (IDE), followed by rinsing in CH_2Cl_2 and air-drying in ambient conditions. The polycorrole coated IDE was placed into a UNIVEX 250 thermal evaporator (Oerlikon, Germany). 50 nm of $LuPc_2$ was deposited under a secondary vacuum of ca. 1.0 x 10^{-6} mbar during the evaporation and keeping the substrate at room temperature. The sublimation of $LuPc_2$ was recorded in the range of 410-420 °C. A glass plate was placed next to the IDEs for the characterization of $LuPc_2$ film. The fundamental electrical and sensing measurements were performed using a Keithley 6517b electrometer with an incorporated DC voltage supply, always at room temperature (20-24°C). The electrometer is controlled by a self-made software via the GP-IB board. Current-voltage (I-V) curves were registered in the range -10 – +10 V, starting and finishing at 0 V bias to avoid irreversible polarization effects [49]. Impedance spectroscopy measurements of the device were recorded on Solartron SI 1260 impedance analyzer interfaced with SMART software. The experiments were performed in a wide frequency range from 10 Hz to 10 MHz, in two different modes. In one case, DC bias is changed in a range from 0 to 10 V at a constant AC bias of 0.2 V. In the other case, AC bias was modulated in the range from 0.05 to 0.5 V at fixed DC bias. The experimental curves were fitted using Zview software.

NH_3 sensing experiments were performed dynamically through alternative exposure to different concentrations of ammonia (in the range 1 to 90 ppm) for either 1 min or 10 min and recovery cycle under clean air for either 4 or 40 min, respectively, at fixed relative humidity (RH) of 40% at fixed bias of 3 V. the required humidity in the chamber was produced through a humidity generator connected with the fluidic lines and was controlled by a commercial humidity sensor (HMT-100, Vaisala, Finland). The system is semiautomated, in which the opening of the mass flow controller valves, mixing of the gases, control of relative humidity (RH) and data acquisition were operated by customized software [50].

Results and discussion

Electropolymerization

The electropolymerization of $CuTpNH_2PC$ on ITO plate was achieved both in 2,6-lutidine/CH_2Cl_2 5/95% v/v + 0.1 M TBAP and in CH_2Cl_2 + 0.1 M TBAP. Two polycorrole coated electrodes were prepared by cycling the potential 20 and 100 times from 0.1 to 0.8 V (Fig. 2a-d), in the presence and in the absence of lutidine.

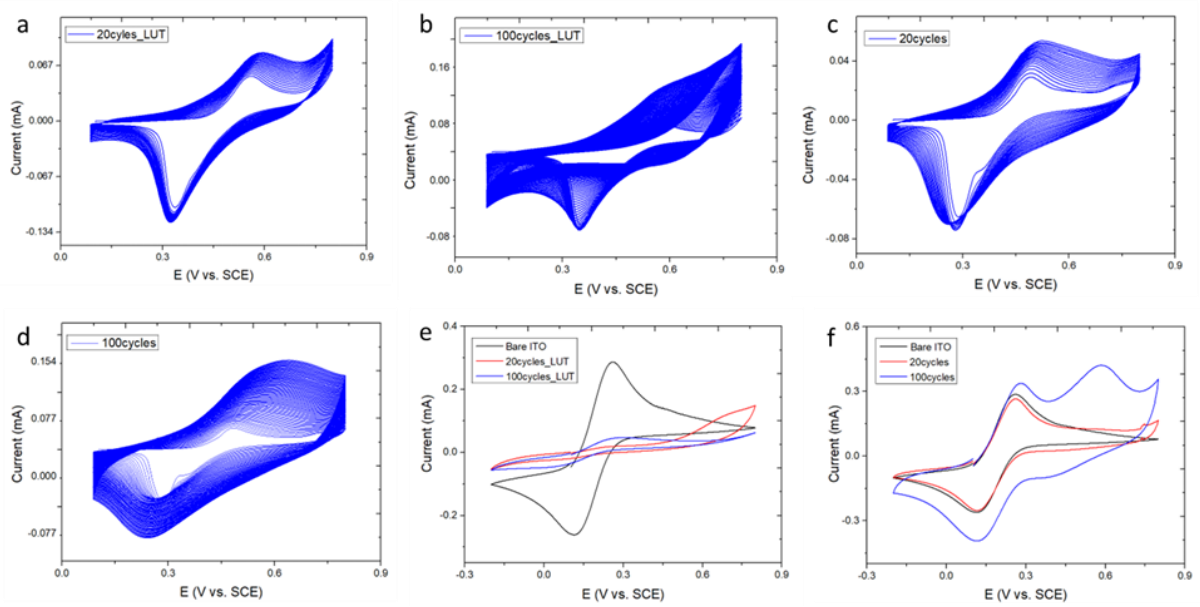

Figure 2. Cyclic voltammograms of 10^{-3} M $CuTpNH_2PC$ with 2,6-lutidine/CH_2Cl_2 5/95% v/v + 0.1 M TBAP in the range 0.1 to 0.8 V at a scan rate of 100 $mV.s^{-1}$ repeated (a) 20 cycles, (b) after 100 cycles and without 2,6-lutidine in CH_2Cl_2 + 0.1 M TBAP (c) 20 cycles, (d) 100 cycles. Voltammograms of 10^{-3} M $K_3[Fe(CN)_6]$ in H_2O + 0.1 M KCl at a bare ITO electrode and ITO modified with $CuTpNH_2PC$ polymer obtained (e) in the presence of 2,6-lutidine and (f) in the absence of lutidine, in the range -0.2 to 0.8 V at 100 $mV.s^{-1}$.

The CVs (Fig. 2a-d) show the continuous increase of the anodic current amplitudes with repeated potential scans and a shift of the anodic peak potential (final E_{pa} = 0.59 V) towards more positive values corresponding to the polymer film formation via the oxidation of $–NH_2$ groups of the $CuTpNH_2PC$ monomer and consecutive coupling to the second monomer molecule. The growing values of anodic current during the first 20 scans indicate the formation of a conductive polymer on ITO glass plate. For the 100 cycles, the shift of the peak potentials is still visible (Fig. 2b and 2d) and it is more pronounced for the polymer obtained without lutidine (final E_{pa} = 0.65 V, Fig. 2d). Even though it was not discussed in the papers reporting

the electropolymerization of cobalt corroles without any base [26,27], it is known that for such oxidative coupling leading to C-C or C-N bonds formation, the rate determining step is the dissociative removal of protons, as demonstrated for the electropolymerization of magnesium porphine [51]. Additionally, without any proton acceptor addition, protonation of polycorrole can occur, leading to an increase in its oxidation potential, and a partial demetallation of the macrocycle, probably due to the protonation of corrole. The electroactivity of the deposited films was investigated by recording the CV in 10^{-3} M $K_3[Fe(CN)_6]$ in the range -0.2 to 0.8 V and compared to the reversible system obtained at the bare electrode (Fig. 2e and 2f). In the presence of 2,6-lutidine, the electrochemical response of $K_3[Fe(CN)_6]$ is very small for the film polymerized with 20 cycles and not visible for the film polymerized with 100 cycles, validating a higher attenuation of the electron transfer, indicating the formation of resistive polymers (Fig. 2e). In contrast, the electrochemical response of $K_3[Fe(CN)_6]$ recorded in the absence of lutidine remains unchanged or even higher compared to that on bare ITO electrode confirming the conducting character of the electrodes modified with polymers prepared without lutidine (Fig. 2f).

Polymer film characterization

The formation of different types of polymer films was confirmed by Raman spectroscopy and by comparison of their spectra with those of the monomer (Fig. 3). For the polymer obtained in the presence of lutidine (Fig. 3a), the weak peak at 823 cm^{-1} provides the evidence of the presence of phenazine groups in the polymer. This skeletal deformation vibration is one of the strongest absorptions in a phenazine spectrum, present in all substituted phenazines [15,52,53]. The peak at 1010 cm^{-1} was attributed to the C-H bond in the phenazine ring, while the polymers exhibit some additional peaks with respect to the monomer at 1142, 1453, and 1525 cm^{-1}, attributed to the phenazine group [54-56]. The peak at 1599 cm^{-1} may be attributed to C-N= vibrations of the phenazine group, due to the higher intensity with respect to the $CuTpNH_2PC$ monomer. Finally, thicker is the polymer film less intense and broader are the peaks, with an apparent disappearance of some peaks, due to a reduction of vibrational degree of freedom in the polymer [14]. For the films electropolymerized in the absence of lutidine, the peaks attributed to the phenazine groups as the characteristic peaks at 1143 and 1453 cm^{-1} are not present (Fig. 3b), although it does

not mean that phenazine units do not form during electropolymerization, but they could be protonated. The main peaks are summarized and assigned in Table S1 [40,57].

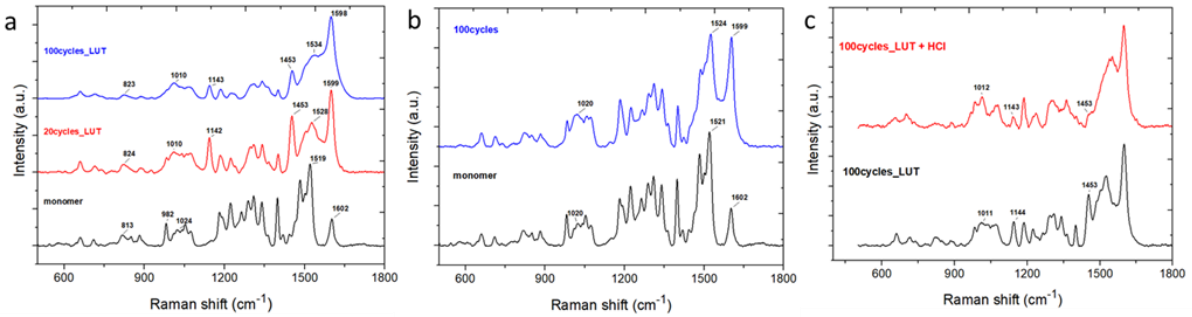

Figure 3. Raman spectrum of $CuTpNH_2PC$ monomer (black line) compared to these of $CuTpNH_2PC$ polymer after 20 cycles (red line) and after 100 cycles (blue line), (a) polymerized in 2,6-lutidine/CH_2Cl_2 5/95% v/v + 0.1 M TBAP, (b) polymerized in CH_2Cl_2 + 0.1 M TBAP. (c) Raman spectrum of $CuTpNH_2PC$ polymer obtained after 100 cycles in 2,6-lutidine/CH_2Cl_2 5/95% v/v + 0.1 M TBAP, before (black line) and after (red line) exposure to HCl vapours.

To confirm this interpretation, we registered Raman spectra of a polymer film obtained with 100 cycles in the presence of 2,6-lutidine before and after 5 min – long exposure to HCl vapors generated from a HCl 37% aqueous solution (Fig. 3c). It is obvious that the two characteristic peaks at 1144 and 1452 cm^{-1} almost disappear after exposure, while all the other peaks remain unchanged. This result clearly demonstrates that the main chemical difference between the two materials is the protonation of polymer chains obtained in the absence of lutidine, the phenazine groups being present in all cases as demonstrated with aminophenylporphyrins [16].

The formation of polymers was also confirmed by comparison of their electronic absorption spectra with the spectrum of the monomer (Fig. 4a and 4b). The spectrum of monomer solution exhibits the characteristic intense Soret band centered at 445 nm with a secondary band at 384 nm and the Q band at 570 nm. These bands are broadened and shifted in the polymer films. The Soret band is shifted at 420 nm and the Q band, depending on the type of polymer, presents different shifts. The evidence of the formation of the polymers is further provided by the XPS analysis of the electrodeposited films and the $Cu(NH_2)TPC$ monomer on ITO substrates. The survey spectra (Fig. 5) show the main elements such as carbon, oxygen, nitrogen and copper at ca 284, 532, 398 and 935 eV, respectively, in the

electrodeposited films and the corrole powder. The intense peak of oxygen in the polymer at 532 eV can be attributed to the adsorption of H_2O on the film surface [58].

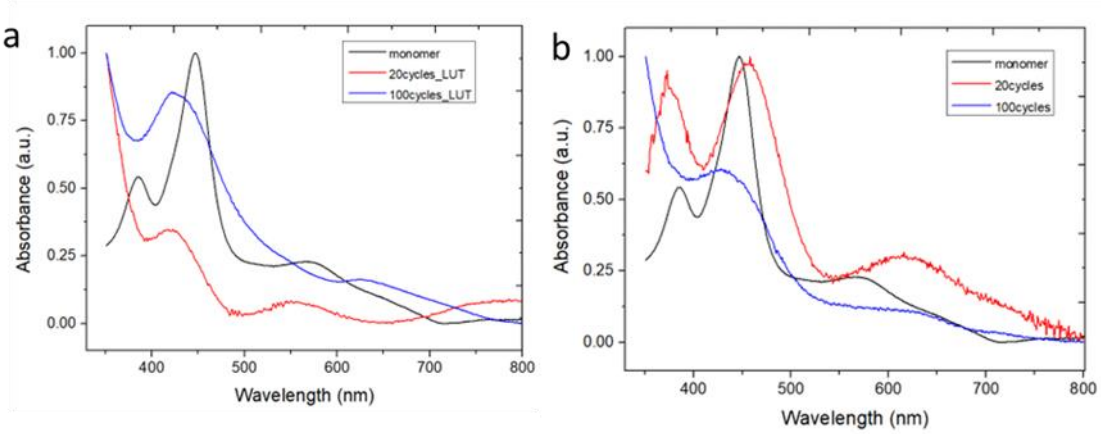

Figure 4. Electronic absorption spectra of $CuTpNH_2PC$ monomer in CH_2Cl_2 solution and polymers on ITO surfaces, obtained in the presence (a) and in the absence (b) of 2,6-lutidine.

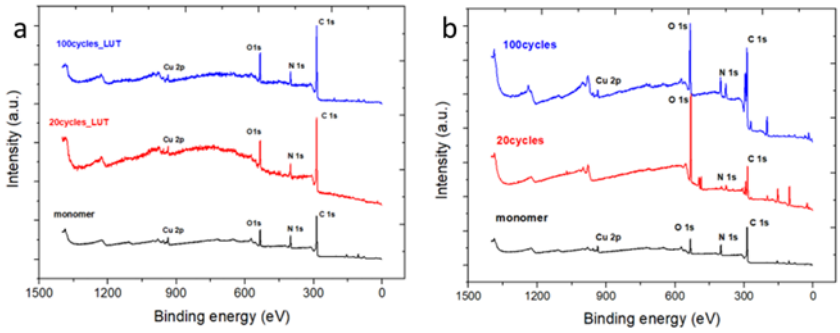

Figure 5. Survey XPS spectra of $CuTpNH_2PC$ monomer (black line) compared to these of polymer films obtained after 20 cycles (red line) and 100 cycles (blue line), (a) in 2,6-lutidine/CH_2Cl_2 5/95% v/v + 0.1 M TBAP and (b) in CH_2Cl_2 + 0.1 M TBAP.

To get deep information about the chemical bonds, high resolution core level XPS spectra were recorded for each element. The N1s spectrum of the corrole monomer (Fig. 6a) shows one peak that can be deconvoluted into two peaks, at 399 and 400 eV, attributed to the metal-nitrogen bonds and the NH_2 groups on the peripheral part of macrocycle [59]. For the polymers obtained in the presence of 2,6-lutidine, the N1s peak attributed to Cu-N bonds remains the more intense and the peak of NH_2 decreases in intensity compared to the monomer, and it is particularly marked for this obtained after 100 cycles (fig. 6c). An additional peak appears as a shoulder at 402 eV, which can be attributed to phenazine rings [56]. The polymers obtained without 2,6-lutidine exhibit very different N1s spectra (Fig. S1), in

particular new peaks appear below 399 eV. Thus, the peak at 397.5 eV can be attributed to pyrrolic N formed because of the corrole demetallation [60], as a result of high local acidity due to the loss of protons during the oxidative coupling reaction [14,51]. The polymer obtained after 20 cycles appears completely demetallated, while the Cu2p signal exists for the polymer film obtained after 100 cycles. The presence of a peak at 396 eV for the polymer obtained after 100 cycles can be attributed to the $–NH^{+}$- group, demonstrating the protonation of these other types of polymers (without lutidine).

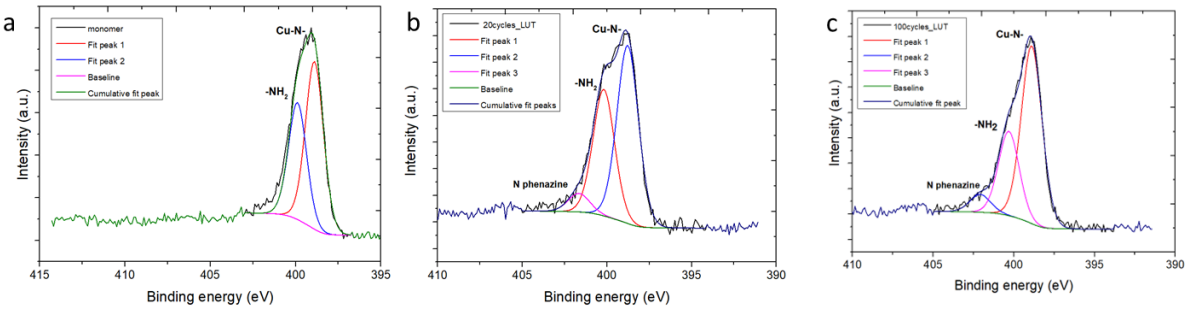

Figure 6. High resolution N1s core-level spectrum of (a) CuTpNH$_2$PC monomer compared to these of polymer films obtained after (b) 20 cycles and (c) 100 cycles, in the presence of 2,6-lutidine.

To obtain a full characterization of the type of binding in the polymer, a ^{1}H NMR was recorded for the monomer and polymer obtained in the presence of 2,6-lutidine after 100 cycles, partially solubilized in $CDCl_3$. The monomer spectrum presents not well-defined peaks due to the paramagnetic behavior of copper ion in the core (Fig. S2). However, it is possible to see the peaks of protons of aromatic rings and pyrrolic protons around 7-8 ppm and the peak around 4 ppm attributed to the NH_2 group on the phenyl rings [47]. The NMR spectrum of the polymer presents more peaks than the monomer. The low concentration makes difficult a wide assignment (Fig. S3). However, the additional peak above 8 ppm and the singlet peak around 7 ppm may be assigned to the protons of the phenazine ring. In addition, around 4 ppm the lack of the peak of the NH_2 group indicates a complete functionalization of the amino groups to form phenazine bonds in the polymer.

Electrical and sensing properties

Polycorrole – based double lateral heterojunction

Electropolymerizing the $CuTpNH_2PC$ monomer was repeated in the same conditions directly on ITO interdigitated electrodes (IDE), both electrodes being covered by the film. Then double lateral heterojunction (DLH) were developed by coating $LuPc_2$ on the polycorrole by thermal evaporation under a secondary vacuum (Fig 7b). We previously reported such DLH devices by electrodepositing polyaniline derivatives [39,61]. Depending on the number of cycles during electropolymerization, 20 or 100, DLH were named 20cycles and 100cycles, for the samples obtained without lutidine and 20cycles_Lut and 100cycles_Lut for the samples obtained in the presence of lutidine, respectively.

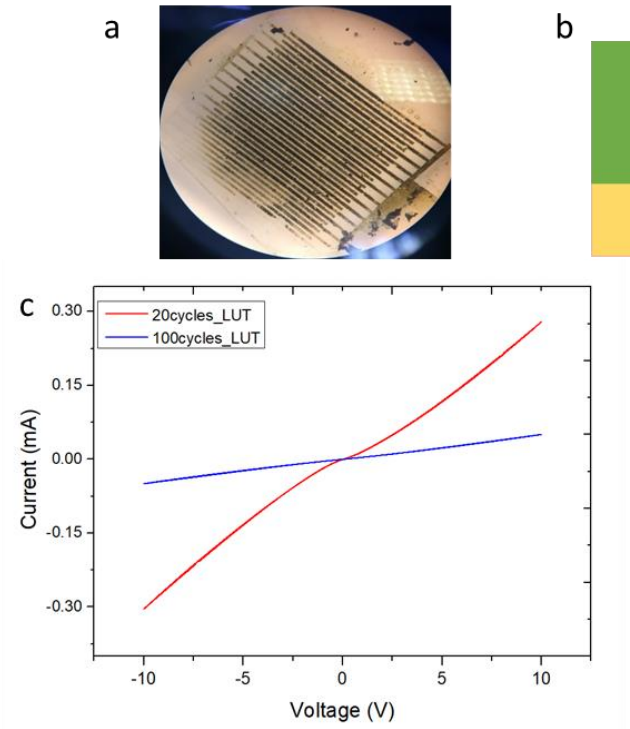

d

Device	I_{+10V} (A)	V_{th} (V)
20cycles_LUT	3×10^{-4}	2.2
100cycles_LUT	6×10^{-5}	1.3 V
20cycles	1.5×10^{-4}	2.2 V
100cycles	1.5×10^{-4}	1.8 V

Figure 7. (a) Optical image of the electropolymerized polycorrole on IDE of ITO on a glass support and (b) scheme of a polycorrole/$LuPc_2$ heterojunction device. (c) I(V) curves of polycorrole/$LuPc_2$ DLH devices with polymers prepared with lutidine, after 20 and 100 cycles. (d) Current values at +10 V and values of the estimated interfacial energy barrier for the four DLH devices.

Electronic absorption spectra of the heterojunction devices clearly show the Q band of $LuPc_2$ at 669 nm (Fig. 8). The second band of $LuPc_2$, at 465 nm, characteristic of its radical nature [2], appears slightly red-shifted in the heterojunction, down to 455 nm, because of its combination with the Soret band of $CuTpNH_2PC$ polymers.

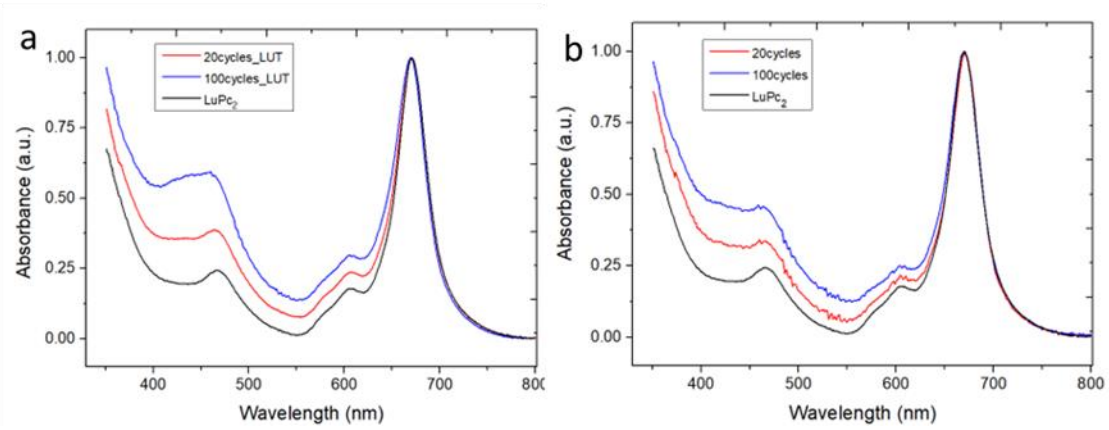

Figure 8. Normalized electronic absorption spectra of the heterojunction devices obtained with 2,6-lutidine (a) and without (b), compared to this of a $LuPc_2$ film deposited on glass.

The electrical properties of devices were investigated by recording the I-V curves in the range from -10 to + 10 V. The non-ohmic feature of the I-V curves in these devices is indicative of the presence of interfacial energy barriers and the accumulation of mobile charges at the polycorrole-$LuPc_2$ interface (Figs. 7c and Fig. S4) [33,40]. The values of the interfacial energy barrier can be estimated by the threshold voltage, V_{th}, determined as the intercept of the tangent to the curve at high bias with the x-axis (Fig. 7d). For all the devices, V_{th} values are close to each other, in the range 1.3 - 2.2 V, which are rather low values for such DLH devices [39,61]. It is worth noting that, for $LuPc_2$ resistors, the I-V curves are perfectly linear, indicating the existence of only ohmic contact between ITO and $LuPc_2$. Another way to compare the devices is their current value at +10 V, which varies from 6 x 10^{-5} A for the polymer prepared with 100 cycles in the presence of lutidine to 1.5 x 10^{-4} A for the two devices prepared without lutidine (Fig. 7d). These current values are rather high, in accordance with the low energy barrier at the interfaces and the high intrinsic conductivity of $LuPc_2$.

The charge transport in DLH devices was further investigated by impedance spectroscopy in a wide frequency range (10 Hz to 10 MHz) at different DC bias between 0-4 V or 0-10 V. The Nyquist plots exhibited different behaviors depending on the type of polymers in the DLH devices (Fig. 9). The device based on polycorrole electrodeposited in 20 cycles with lutidine (20cycles_Lut) displayed two depressed semicircles (Fig. 9a) in which the one at high frequency (HF, left part) remains unchanged whatever the applied DC bias, while the one at low frequency (LF, right part) decreases as a function of increasing DC bias and almost

disappears around 3 V. The former characterizes the bulk transport in the device and is therefore independent of the bias. The latter corresponds to the interfacial transport that becomes easier when increasing the bias leading to a decrease of the LF semicircle. The same behavior was observed for the 20cycles device obtained without lutidine (Fig. 9c). The semicircle in the LF region of the Nyquist plots corresponds to the charge transport at the interface of the organic-organic junction. At low DC bias, the charges injected from the electrode encounter larger resistance in the relatively low conducting sublayer to arrive at the interface. Thus, only a small number of mobile carriers arrive at the interface, resulting in the highly resistive interfacial transport, which explains the appearance of the larger semicircle at 0 V. However, at higher bias, electric field intensity increases, which propels larger mobile charge carriers to arrive at the interface, populating the interface region with mobile charges and facilitating the faster interfacial charge transport. Consequently, the interfacial resistance decreases and the associated semicircle in the Nyquist plot becomes smaller. It can be remarked that the decrease in the semicircle attenuates at higher bias, which is attributed to the saturation of the injected charges arrival from the electrode to the interface. The devices with polycorroles obtained in 100 cycles show the same Nyquist plots whatever the presence (Fig. 9b) or absence (Fig. 9d) of lutidine. An important HF semicircle is observed, while the LF semicircle, very low, appears only for low values of the DC bias and merges with that at HF when increasing the bias. It indicates the prevalence of only bulk transport and the very low interface effect, in agreement with the electrodeposition of thicker films. This is confirmed by the maximum resistance, ca. $5x10^5$ Ω (Re(Z)), compared to only $6x10^4$ Ω for the 20cycles_Lut DLH device. The Nyquist plots were modeled by Constant Phase Element (CPE) based equivalent circuits. It is assumed that the distributed microstructural properties of the heterostructure is an imperfect capacitor [62] in which its impedance Z_{CPE} is given by equation (1).

$$Z_{CPE_i} = \frac{1}{Q_i \times (j\omega)^{\alpha_i}} \qquad (1)$$

where Q_i is the non-ideal capacitance, ω the frequency ($2\pi f$) and α_i a coefficient changing between 0 and 1 such that its upper and lower limits correspond to an ideal capacitor and an ideal resistor, respectively.

The Nyquist plots were fitted with an equivalent circuit having two Ri-CPEi elements arranged in series (Inset of Fig. 9a); the semicircle at HF is described by bulk resistance R1 and CPE1, while that at LF is simulated with interfacial resistance R2 and CPE2. The different

parameters of the equivalent circuit, such as the resistance (*Ri*), α and the effective capacitance (*Cieff*, equation (2)) were determined.

$$C_{ieff} = Q_i^{\frac{1}{\alpha_i}} \times R_i^{\frac{1}{\alpha_i}} \qquad (2)$$

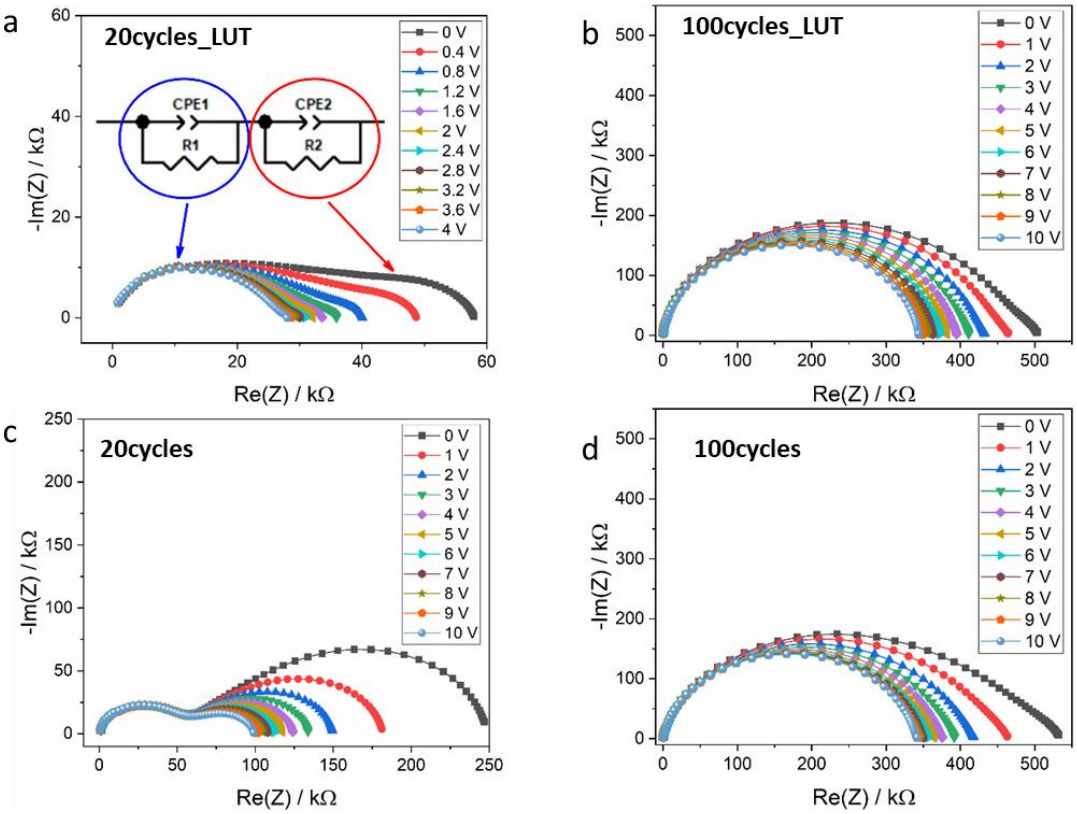

Figure 9. Impedance spectra recorded in the range of 10 to 10 MHz at different bias (0 to 4 V or 0 to 10 V) and at fixed AC bias of 0.2 V, for DLH devices with polymers prepared with lutidine, with (a) 20 and (b) 100 cycles, and without, with (c) 20 and (d) 100 cycles.

Their variations with DC bias are shown in Fig. S5. The devices based on polycorrole electrodeposited in 20 cycles (Figs. S5a and S5d) exhibit decrease in R2 from ca. 36 kΩ to 7 kΩ as bias changes from 0 to 4 V and from 213 kΩ to 50 kΩ as bias changes from 0 to 10 V with and without lutidine, respectively. Both devices present almost no change in R1 with values ca. 21 kΩ and 50 kΩ respectively. When the polycorrole was electrodeposited in 20 cycles (Figs. S5a and S5d), most of decrease in R2 takes place until 2 V and until 3 V with and without lutidine, respectively. It indicates that injected charges encounter an energy barrier of approximately 2 V and 3 V, respectively, to reach more conducting interface region. It is in agreement with the V_{th} value (2.2 V) obtained from the I-V curve. On the other hand, charge

transfer resistances in DLH devices realized with polycorroles electrodeposited in 100 cycles (Figs. S5g and S5j) remain nearly constant at different bias, typical for a bulk transport. The $\alpha 1$ values remain close to 1 whatever the bias and the device, indicating that the bulk component behaves close to an ideal capacitor owing to the homogeneous microstructure of the bulk. However, while $\alpha 2$ remains around 0.9 for the 100 cycles polymers, it falls to 0.6-0.7 for the 20 cycles polycorroles indicating dispersion in the CPE, which is attributed to enhancement in surface heterogeneity at the interface of 20 cycles – based heterojunctions.

Analysis of the variations of the effective capacitances (Figs. S5g,f,i,l) allows understanding the interface effect on the charge transport in the DLH devices. When polycorroles were electrodeposited in 20 cycles (Figs. S5g,f), the *C2eff* values corresponding to the polymer-$LuPc_2$ interface decrease slightly from 35 nF to 20 nF and from 28 nF to 12 nF, with and without lutidine, respectively, as DC increases, but remains 3-order of magnitude higher than the bulk capacitance (*C1eff*). It confirms the accumulation of charges (e^- and h^+) at the interface of the heterojunctions. When polycorroles were electrodeposited in 100 cycles (Figs. S5i,l), the *C2eff* values are close to the bulk ones (*C1eff*), i.e. 3-order of magnitude lower than those of DLH devices realized with polycorroles electrodeposited in 20 cycles. It confirms the absence of significant interface effect in the device, and it is in agreement with an increase of the thickness of the layer, since capacitance is inversely proportional to the thickness.

Ammonia sensing

The ammonia sensing properties of the different DLH devices were investigated at first by applying alternate exposure to 90 ppm of NH_3 (10 min) and recovery under clean air (30 min), at a fixed relative humidity value. The devices obtained in the presence of lutidine exhibit a current decrease under ammonia (Fig. 10), indicating that charge transport is dominated by positive majority charge carriers, ammonia being an electron-donating species. It was expected, since the corrole does not bear any withdrawing substituents and $LuPc_2$ behaves also as a p-type material in air. The device obtained with 20 cycles exhibits a rather stable response when exposed to short exposure/recovery cycles (1 min/4 min), which is dependent on the ammonia concentration in the range 10-90 ppm. The device prepared with 100 cycles shows an important drift of the baseline current. However, the response at 90 ppm remains

the same at the end of the experiment compared to the first exposure period at the same concentration (Fig. 10c). The relative response, RR(%) = (I_f - I_i) x 100)/I_i, was calculated to be 0.2%/ppm and 0.1%/ppm for the polymers obtained with 20 and 100 cycles, respectively (Table 1), I_f and I_i being the current values at the end and at the beginning of an exposure period, respectively. An additional point to mention is current increase observed at 10 ppm of NH_3 exposure for the polycorrole film prepared with 100 cycles, even though it remains very small, which suggests a n-type behaviour. This behaviour could result from an interaction of NH_3 molecules with a few protonated sites present in the polymer.

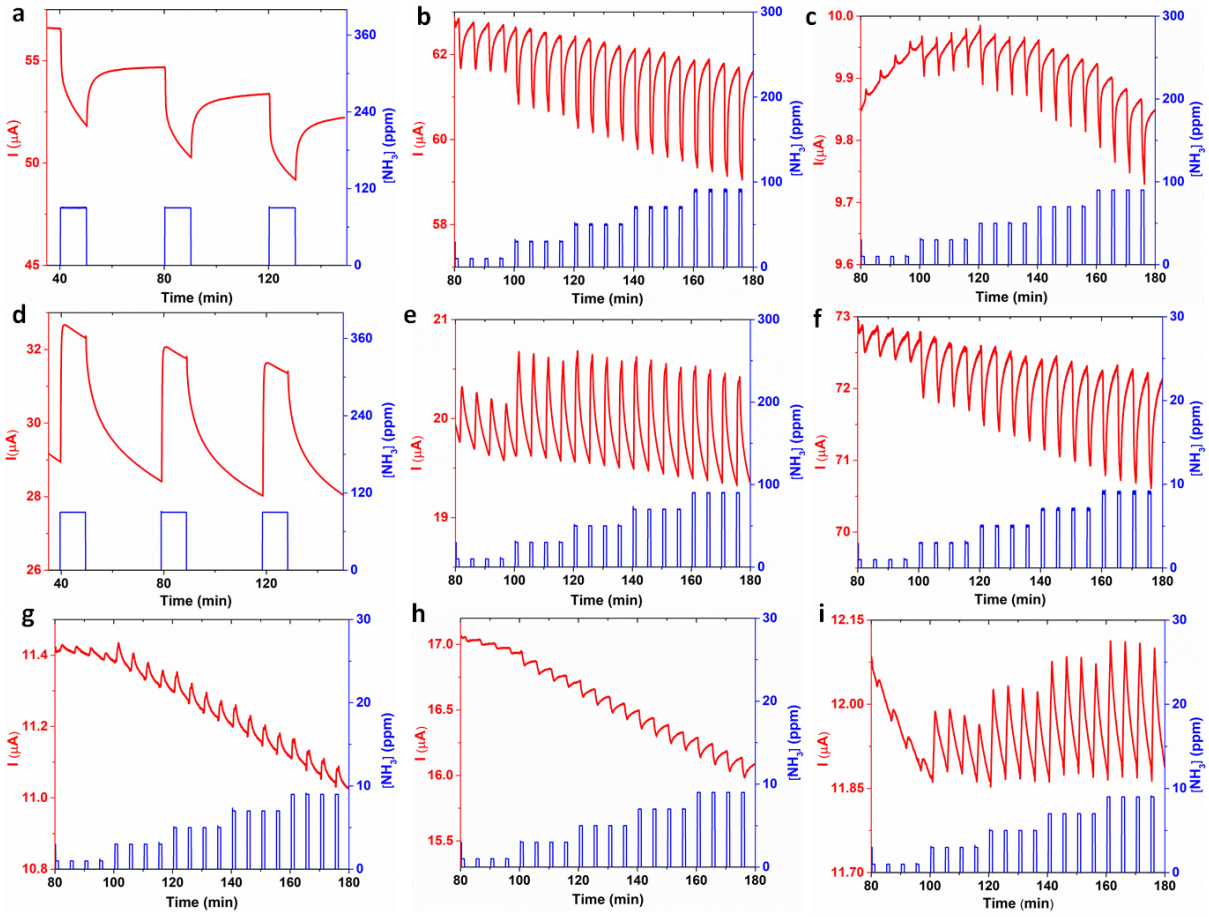

Figure 10. Current variation as a function of time for DLH devices obtained when exposed to 90 ppm NH_3 (10 min/30 min exposure-recovery cycles) for the polymer obtained with lutidine (a) 20 cycles and without (d) 100cycles. Response curve at variable NH_3 concentrations in the range 10-90 ppm during 1 min/4 min exposure/recovery cycles, for polymer obtained with (b) 20 cycles and (c) with 100 cycles in presence of lutidine and without (e) with 100 cycles . Current variation as a function of time for DLH devices obtained with lutidine (f) 20cycles and (g) 100cycles and without (h) 20cycles and (i) 100cycles, when exposed to variable NH_3 concentrations in the range 1-9 ppm during 1 min/4 min exposure/recovery cycles. All measurements were carried out at a bias of 3 V and at a RH value of 40%.

To confirm this point, we studied DLH devices prepared with 100 cycles in the absence of lutidine, which contain highly protonated polycorrole (Figs. 10d and 10e). Whatever the ammonia concentration and whatever the duration of the exposure/recovery cycles, current increases under NH_3, showing the n-type behaviour of these devices, with a response depending on its concentration. We can explain this opposite behaviour compared to the previous devices by the high protonation level of polymer chains that act as electro-withdrawing groups for the corrole units in which electrons can be easily injected. Since the responses of the sensors were sufficiently high and repeatable at 10 ppm, sensors behaviour was further investigated at lower concentrations (1-9 ppm) to evaluate the experimental detection threshold. The response curves of the different DLH sensors are presented in Figs. 10f-i. Each of the sensors displays the similar qualitative behaviour as noticed in higher NH_3 concentration ranges between 10 to 90 ppm, namely a negative response to NH_3 for the DLH obtained with 20 cycles in the presence of lutidine (Fig. 10f) and a positive response for both devices prepared with 100 cycles, with (Fig. 10g) and without (Fig. 10i) lutidine. In terms of stability of the baseline, the device prepared with 20 cycles in the presence of lutidine is better, while the two other devices exhibit a drift, but with responses at a given concentration identical under decreasing or increasing ammonia concentrations. Notably, the drift in the different DLH sensors baseline signal can arise from a complex phenomenon, which can be attributed to multiple parameters. It mainly includes incomplete desorption and diffusion of the gas molecules, which are further affected by the temperature, humidity and the sensing film morphologies. These effects are further compounded, while performing sensing studies at low gas concentration, because even a small drift induced by incomplete desorption or diffusion can be of similar magnitude as of the sensor signal variation upon gas adsorption.

In Figure 11, calibration curves of the different DLH sensors are presented, depicting RR variation as a function of NH_3 concentration. The calibration curves of the different sensors evidence a rapid increase at lower concentration followed by a saturation in the response at higher concentration. Such behaviour is typical in gas sensors, which are attributed to the limited number of sensor active sites, which saturate at the higher gas concentration. In the DLH sensor containing polycorrole layer prepared in the absence of lutidine, response is positive and the magnitude of the sensor response being proportional to the thickness of polycorrole. On the other hand, sensor based on polycorrole prepared in the presence of

lutidine exhibits negative response towards NH_3 and RR is inversely proportional to the thickness of the polycorrole layer in the heterostructure.

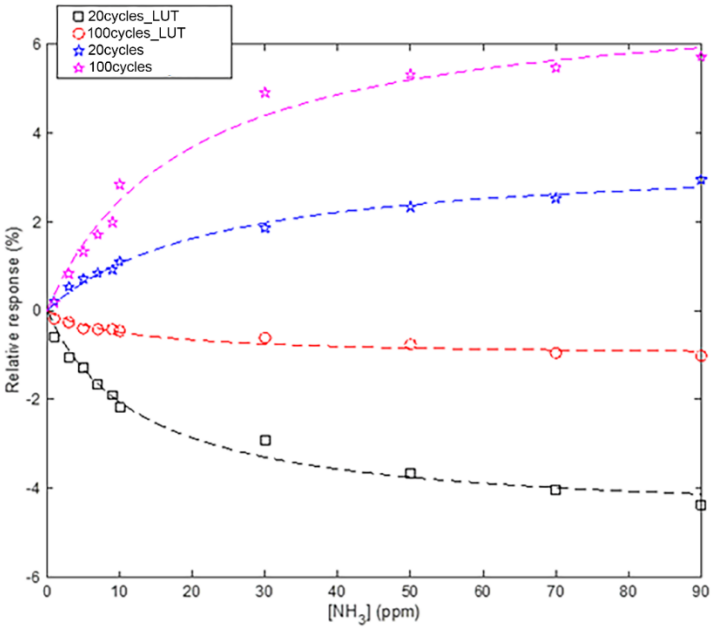

Figure 11. Relative response as a function of NH_3 for all devices, in the range 1-90 ppm, in air, at 40 % RH, during exposure/ recovery cycles (1 min/4 min).

Such contrasting features of the calibration curves variation can be explained by the different regimes of gas material interactions and charge transport process. Accordingly, the polycorroles layer coated in the absence of lutidine remain positively charged, which favours the diffusion of electron donating NH_3 into the bulk of the sublayer. Thus, increase in the sensor response in the thicker polycorrole containing DLH sensor can be assigned to the higher diffusion contribution. On the contrary, the polycorrole layer deposited in the presence of lutidine is not positively charged, which minimizes the diffusion of NH_3 in the bulk of the sublayer and the interaction is mainly dominated by surface adsorption. In such case, charge transport plays an important role towards NH_3 sensing response. Here, a thicker polycorrole layer, deposited at 100 cycles impart a highly resistive bulk region, making the charge transfer from the electrode to the interface difficult. This can explain the lower response of the DLH sensor containing polycorrole prepared at 100 cycles compared to the one having polycorrole film deposited for 20 cycles. Thus, different profiles of the calibration curves clearly manifest the influence of polycorrole composition on the NH_3 sensing behaviour. The calibration curves are further fitted with a Langmuir isotherm function (equation (3)).

$$RR = RR_{max} \frac{c}{K+C} \qquad (3)$$

where RR_{max} is the asymptotic response and K is the affinity parameter defined as the concentration at which half of the asymptotic response is achieved. The results of the fit are shown in Table 1.

Table 1. Langmuir function fit parameters, coefficient of determination (R^2), the calculated sensitivity at the origin, and the estimated limit of detection

Sensor	RR_{max} (%)	K (ppm)	R^2	S(c=0) (%/ppm)	LOD (ppb)
20 cycles Lut	-4.72	12.9	0.97	-0.36	128
100 cycles Lut	-1.03	11.1	0.91	-0.09	513
20 cycles	+3.46	22.7	0.98	+0.15	308
100 cycles	+7.15	18.9	0.98	+0.37	125

From Table 1, it is evident that besides influencing the magnitude of the sensor response, the formulation of polycorrole also affects the affinity parameter, which changes with the thickness of polycorrole and the amount of positive charges in it. The limit of detection can be estimated as the ratio between the uncertainty of the relative response (ΔRR) and the absolute value of the sensitivity at the origin. The sensitivity at the origin has been estimated as the derivative of the Langmuir function at c=0. The sensitivity of the four sensors is shown in table 1. The uncertainty of the relative response can be calculated from the baseline current signal-to-noise (S/N) ratio (equation (4)).

$$\Delta RR = 100 \cdot \frac{2}{S/N} \qquad (4)$$

The measured S/N ratio is of the order of $1 \cdot 10^4$. The estimated LODs are shown in table 1. The DLH of $LuPc_2$ and polycorrole show an improvement of performance respect to other previously studied DLH sensors. Devices made of $LuPc_2$ and poly-2,5-dimethoxyaniline (PDMA) [39] and with perfluoropolyaniline (PTFA) [61], and perfluoro- copper phthalocyanine ($Cu(F_{16}Pc)$) – based heterojunctions achieved a LOD of the order of 314 ppb, 450 ppb, and 280 ppb respectively. A similar performance with a LOD of 140 ppb was obtained with $Cu(F_{16}Pc)$, but after the tuning of the work function of the ITO electrode achieved with a layer of electrografted 2,5-dimethoxybenzene between the ITO electrode and $Cu(F_{16}Pc)$ [38].

Conclusion

A copper complex of the 5,10,15-tris(4-aminophenyl)corrole has been electropolymerized for the first time onto ITO electrodes. Cycling the applied potential from 0.1 to 0.8 V affords conductive corrole polymers, with the film thickness tuned by the number of cycles (20 or 100). The polymerization proceeds through the formation of phenazine groups among the peripheral 4-aminophenyl substituents of the corrole monomers. However the polymerization conditions strongly influenced the nature of the final products: when the reaction was carried in neat CH_2Cl_2, the lack of proton acceptors led to the fully protonation of the polymer chains, as evidenced by the spectroscopic characterization of the final polymers. Moreover, the acidic conditions induced also the partial demetallation of the macrocycles. These side reactions can be avoided by the addition of lutidine to the electropolymerization media; in this case, the presence of the base prevented the loss of the coordinated copper, although for the 100 cycling a partial protonation was still present.

These differences greatly influenced the ammonia sensing properties of the polycorroles when they are exploited as inner layers coated with $LuPc_2$ in DLH devices. The protonation of the polymer chains, in fact, induces a n-type behaviour of the double layer heterojunction devices. The partial protonation of the polycorrole obtained with 100 cycles in the presence of lutidine reduces the responses of the resulting device, with an inversion among p- and n-type behaviour observed for the low ammonia concentrations. The DLH obtained with 20 cycles with lutidine exhibits a p-type behaviour with the highest sensitivity that favorably competes with these reported so far for DLH heterojunctions.

In this work we demonstrate the possibility to tune the sensing properties of the polycorroles by simple synthetic procedures; this possibility is particularly appealing for the preparation of optimized devices and further studies are now in progress in our laboratories in this direction.

Acknowlegments

The authors acknowledge the Agence Nationale de la Recherche for funding through the ANR project OUTSMART ANR-2015-CE39-0004-03. This research was funded by the European Union through the Fonds Européen de Développement Régional (FEDER) and the Conseil régional Bourgogne Franche-Comté through both the PIA-excellence ISITE-BFC PO FEDERFSE Bourgogne 2014-2020 via the CoMICS program, Chemistry of Molecular Interactions Catalysis

and Sensors, and the Envergure Program MatElectroCap (2020-2024). The Italian Ministry of Education, University and Research (MIUR) is thanked for the PRIN project SUNSET (R. P., Grant 2017EKCS35_002). The authors thank the Plateforme d'Analyses Chimiques et de Synthèse Moléculaire de l'Universite de Bourgogne (PACSMUB) and the SATT Sayens for technical support in the Raman analyses. A. K. acknowledges the Université de Bourgogne for a postdoctoral fellowship through the BQR program.

References

[1] D. Dini, M. Hanack, Physical properties of phthalocyanine-based materials, in: K.M. Kadish, K.M. Smith, R. Guilard (Eds.), The Porphyrin Handbook, Academic Press, Cambridge, 2003: Vol. 17, pp. 1–36.

[2] M. Bouvet, Radical phthalocyanines and intrinsic semiconduction, in: K.M. Kadish, K.M. Smith, R. Guilard (Eds.), The Porphyrin Handbook, Academic Press, Cambridge, 2003: Vol. 19, pp. 37–103.

[3] O.A. Melville, B.T.H. Lessard, T.P. Bender, Phthalocyanine-Based Organic Thin-Film Transistors: A Review of Recent Advances, ACS Appl. Mater. Interfaces. 7 (2015) 13105–13118. doi:10.1021/acsami.5b01718.

[4] G. de la Torre, G. Bottari, T. Torres, Phthalocyanines and Subphthalocyanines: Perfect Partners for Fullerenes and Carbon Nanotubes in Molecular Photovoltaics, Adv. Energy Mater. 7 (2017) 1601700. doi:10.1002/aenm.201601700.

[5] R. Paolesse, S. Nardis, D. Monti, M. Stefanelli, C. Di Natale, Porphyrinoids for Chemical Sensor Applications, Chem. Rev. 117 (2017) 2517–2583. doi:10.1021/acs.chemrev.6b00361.

[6] D. Wörhrle, G. Schnurpfeil, Porphyrins and phthalocyanines in macromolecules, in: K.M. Kadish, K.M. Smith, R. Guilard (Eds.), The Porphyrin Handbook, Academic Press, Cambridge, 2003: Vol. 17, pp. 177–246.

[7] W. Ji, T.-X. Wang, X. Ding, S. Lei, B.-H. Han, Porphyrin- and phthalocyanine-based porous organic polymers: From synthesis to application, Coord. Chem. Rev. 439 (2021) 213875. doi:10.1016/j.ccr.2021.213875.

[8] A. Osuka, H. Shimidzu, meso, meso-Linked Porphyrin Arrays, Angew. Chem. Int. Ed. Engl. 36 (1997) 135–137. doi:10.1002/anie.199701351.

[9] T. Tanaka, A. Osuka, Conjugated porphyrin arrays: synthesis, properties and applications for functional materials, Chem. Soc. Rev. 44 (2015) 943–969. doi:10.1039/C3CS60443H.

[10] A. Tsuda, H. Furuta, A. Osuka, Completely Fused Diporphyrins and Triporphyrin, Angew. Chem. Int. Ed. Engl. 39 (2000) 2549–2552. doi:10.1002/1521-3773(20000717)39:14<2549::AID-ANIE2549>3.0.CO;2-A.

[11] F. Bedioui, J. Devynck, C. Bied-Charreton, Immobilization of Metalloporphyrins in Electropolymerized Films: Design and Applications. *Acc. Chem. Res. 28 (1995)* 30–36. doi.org/10.1021/ar00049a005.

[12] M.A. Vorotyntsev, D.V. Konev, C.H. Devillers, I. Bezverkhyy, O. Heintz, Magnesium(II) polyporphine: The first electron-conducting polymer with directly linked unsubstituted porphyrin units obtained by electrooxidation at a very low potential, Electrochim. Acta. 55 (2010) 6703–6714. doi:10.1016/j.electacta.2010.06.001.

[13] M.A. Vorotyntsev, D.V. Konev, C.H. Devillers, I. Bezverkhyy, O. Heintz, Electroactive polymeric material with condensed structure on the basis of magnesium(II)

polyporphine, Electrochim. Acta. 56 (2011) 3436–3442. doi:10.1016/j.electacta.2010.10.039.
[14] A. Kumar, N. Alami Mejjati, R. Meunier-Prest, A. Krystianiak, O. Heintz, E. Lesniewska, et al., Tuning of interfacial charge transport in polyporphine/phthalocyanine heterojunctions by molecular geometry control for an efficient gas sensor, Chem. Eng. J. 429 (2022) 132453. doi:10.1016/j.cej.2021.132453.
[15] M.G. Walter, C.C. Wamser, Synthesis and Characterization of Electropolymerized Nanostructured Aminophenylporphyrin Films, J. Phys. Chem. C. 114 (2010) 7563–7574. doi:10.1021/jp910016h.
[16] N.U. Day, M.G. Walter, C.C. Wamser, Preparations and Electrochemical Characterizations of Conductive Porphyrin Polymers, J. Phys. Chem. C. 119 (2015) 17378–17388. doi:10.1021/acs.jpcc.5b02628.
[17] A. Ghosh, Electronic Structure of Corrole Derivatives: Insights from Molecular Structures, Spectroscopy, Electrochemistry, and Quantum Chemical Calculations, Chem. Rev. 117 (2017) 3798–3881. doi:10.1021/acs.chemrev.6b00590.
[18] S. Nardis, F. Mandoj, M. Stefanelli, R. Paolesse, Metal complexes of corrole, Coord. Chem. Rev. 388 (2019) 360–405. doi:10.1016/j.ccr.2019.02.034.
[19] A.W. Johnson, I.T. Kay, 306. Corroles. Part I. Synthesis, J. Chem. Soc. (1965) 1620–1629.
[20] R. Paolesse, S. Mini, F. Sagone, T. Boschi, L. Jaquinod, D.J. Nurco, et al., 5,10,15-Triphenylcorrole: a product from a modified Rothemund reaction, Chem. Commun. (1999) 1307–1308. doi:10.1039/A903247I.
[21] Z. Gross, N. Galili, I. Saltsman, The First Direct Synthesis of Corroles from Pyrrole, Angew. Chem. Int. Ed. Engl. 38 (1999) 1427–1429. doi:10.1002/(SICI)1521-3773(19990517)38:10<1427::AID-ANIE1427>3.0.CO;2-1.
[22] C. Di Natale, C.P. Gros, R. Paolesse, Corroles at work: a small macrocycle for great applications, Chem. Soc. Rev. 51 (2022) 1277–1335. doi:10.1039/d1cs00662b.
[23] Z. Gross, H.B. Gray, Oxidations Catalyzed by Metallocorroles, Advanced Synthesis & Catalysis. 346 (2004) 165–170. doi:10.1002/adsc.200303145.
[24] R.D. Teo, J.Y. Hwang, J. Termini, Z. Gross, H.B. Gray, Fighting Cancer with Corroles, Chem. Rev. 117 (2017) 2711–2729. doi:10.1021/acs.chemrev.6b00400.
[25] N. Levy, A. Mahammed, A. Friedman, B. Gavriel, Z. Gross, L. Elbaz, Metallocorroles as Non-Precious Metal Electrocatalysts for Highly Efficient Oxygen Reduction in Alkaline Media, ChemCatChem. 8 (2016) 2832–2837. doi:10.1002/cctc.201600556.
[26] A. Friedman, I. Saltsman, Z. Gross, L. Elbaz, Electropolymerization of PGM-free molecular catalyst for formation of 3D structures with high density of catalytic sites, Electrochim. Acta. 310 (2019) 13–19. doi:10.1016/j.electacta.2019.04.096.
[27] A. Friedman, L. Landau, S. Gonen, Z. Gross, L. Elbaz, Efficient Bio-Inspired Oxygen Reduction Electrocatalysis with Electropolymerized Cobalt Corroles, ACS Catalysis. 8 (2018) 5024–5031. doi:10.1021/acscatal.8b00876.
[28] S. Ooi, T. Tanaka, K.H. Park, S. Lee, D. Kim, A. Osuka, Fused Corrole Dimers Interconvert between Nonaromatic and Aromatic States through Two-Electron Redox Reactions, Angew. Chem. 127 (2015) 3150–3154. doi:10.1002/ange.201411242.
[29] C. Di Natale, A. Macagnano, E. Martinelli, R. Paolesse, G. D'Arcangelo, C. Roscioni, et al., Lung cancer identification by the analysis of breath by means of an array of non-selective gas sensors, Biosensors and Bioelectronic. 18 (2003) 1209–1218. doi:10.1016/s0956-5663(03)00086-1.

[30] L. Tortora, G. Pomarico, S. Nardis, E. Martinelli, A. D'Amico, C. Di Natale, et al., Supramolecular sensing mechanism of corrole thin films, Sens. Actuators: B. Chem. 187 (2013) 72–77. doi:10.1016/j.snb.2012.09.055.
[31] M. Vanotti, S. Poisson, V. Soumann, V. Quesneau, S. Brandès, N. Desbois, et al., Influence of interfering gases on a carbon monoxide differential sensor based on SAW devices functionalized with cobalt and copper corroles, Sens. Actuators: B. Chem. 332 (2021) 129507. doi:10.1016/j.snb.2021.129507.
[32] A. Kumar, R. Meunier-Prest, M. Bouvet, Organic Heterojunction Devices Based on Phthalocyanines: A New Approach to Gas Chemosensing, Sensors. 20 (2020) 4700–. doi:10.3390/s20174700.
[33] H. Wang, D. Yan, Organic heterostructures in organic field-effect transistors, NPG Asia Mater. 2 (2010) 69–78. doi:10.1038/asiamat.2010.44.
[34] S. Ji, H. Wang, T. Wang, D. Yan, A High-Performance Room-Temperature NO2 Sensor Based on An Ultrathin Heterojunction Film, Adv. Mater. 25 (2013) 1755–1760. doi:10.1002/adma.201204134.
[35] H. Fan, W. Shi, X. Yu, J. Yu, High performance nitrogen dioxide sensor based on organic field-effect transistor utilizing ultrathin CuPc/PTCDI-C8 heterojunction, Synth. Met. 211 (2016) 161–166. doi:10.1016/j.synthmet.2015.11.021.
[36] G. Bengasi, R.M. Prest, K. Baba, A. Kumar, A.L. Pellegrino, N.D. Boscher, et al., Molecular Engineering of Porphyrin-Tapes/Phthalocyanine Heterojunctions for a Highly Sensitive Ammonia Sensor, Adv. Electron. Mater. 6 (2020) 2000812. doi:10.1002/aelm.202000812.
[37] M. Bouvet, J. Simon, Electrical properties of rare earth bisphthalocyanine and bisnaphthalocyanine complexes, Chem. Phys. Lett. 172 (1990) 299–302. doi:10.1016/0009-2614(90)85407-4.
[38] M. Mateos, R. Meunier-Prest, J.-M. Suisse, M. Bouvet, Modulation of the organic heterojunction behavior, from electrografting to enhanced sensing properties, Sens. Actuators: B. Chem. 299 (2019) 126968.
[39] M. Mateos, M.-D. Tchangaï, R. Meunier-Prest, O. Heintz, F. Herbst, J.-M. Suisse, et al., Low Conductive Electrodeposited Poly(2,5-dimethoxyaniline) as a Key Material in a Double Lateral Heterojunction, for Sub-ppm Ammonia Sensing in Humid Atmosphere, ACS Sens. 4 (2019) 740–747. doi:10.1021/acssensors.9b00109.
[40] S. Ouedraogo, R. Meunier-Prest, A. Kumar, M. Bayo-Bangoura, M. Bouvet, Modulating the Electrical Properties of Organic Heterojunction Devices Based On Phthalocyanines for Ambipolar Sensors, ACS Sens. 5 (2020) 1849–1857. doi:10.1021/acssensors.0c00877.
[41] Z. Sahin, R. Meunier-Prest, F. Dumoulin, A. Kumar, U. Isci, M. Bouvet, Tuning of organic heterojunction conductivity by the substituents' electronic effects in phthalocyanines for ambipolar gas sensors, Sens. Actuators: B. Chem. 332 (2021) 129505. doi:10.1016/j.snb.2021.129505.
[42] A. Kumar, R. Meunier-Prest, E. Lesniewska, M. Bouvet, Interplay of electrode geometry and bias on charge transport in organic heterojunction gas sensors, Sens. Actuators: B. Chem. 369 (2022) 132313. doi:10.1016/j.snb.2022.132313.
[43] B. Timmer, W. Olthuis, A.V.D. Berg, Ammonia sensors and their applications—a review, Sens. Actuators: B. Chem. 107 (2005) 666–677. doi:10.1016/j.snb.2004.11.054.
[44] C. Di Natale, R. Paolesse, E. Martinelli, R. Capuano, Solid-state gas sensors for breath analysis: A review, Anal. Chim. Acta. 824 (2014) 1–17. doi:10.1016/j.aca.2014.03.014.

[45] O. Tsuboi, S. Momose, R. Takasu, Mobile Sensor that Quickly and Selectively Measures Ammonia Gas Components in Breath, Fujitsu Scientific & Technical Journal. 53 (2017) 38–43.
[46] P. Turek, P. Petit, J.-J. André, J. Simon, R. Even, B. Boudjema, et al., A new series of molecular semiconductors: phthalocyanine radicals, J. Am. Chem. Soc. 109 (1987) 5119–5122. doi:10.1021/ja00251a012.
[47] R. Paolesse, S. Nardis, F. Sagone, R.G. Khoury, Synthesis and Functionalization of meso-Aryl-Substituted Corroles, J. Org. Chem. 66 (2001) 550–556. doi:10.1021/jo005661t.
[48] C. Clarisse, M.T. Riou, Synthesis and characterization of some lanthanide phthalocyanines, Inorg. Chim. Acta. 130 (1987) 139–144. doi:10.1016/S0020-1693(00)85943-5.
[49] A. Kumar, R. Meunier-Prest, F. Herbst, O. Heintz, E. Lesniewska, M. Bouvet, Covalent grafting of aryls to modulate the electrical properties of phthalocyanine-based heterostructures: Application to ammonia sensing, Chem. Eng. J. 436 (2022) 135207. doi:10.1016/j.cej.2022.135207.
[50] P. Gaudillat, A. Wannebroucq, J.-M. Suisse, M. Bouvet, Bias and humidity effects on the ammonia sensing of perylene derivative/lutetium bisphthalocyanine MSDI heterojunctions, Sens. Actuators: B. Chem. 222 (2016) 910–917. doi:10.1016/j.snb.2015.09.015.
[51] D.V. Konev, C.H. Devillers, K.V. Lizgina, V.E. Baulin, M.A. Vorotyntsev, Electropolymerization of non-substituted Mg(II) porphine: Effects of proton acceptor addition, J. Electroanal. Chem. 737 (2015) 235–242. doi:10.1016/j.jelechem.2014.09.018.
[52] C. Stammer, A. Taurins, Infrared spectra of phenazines, Spectrochim. Acta. 19 (1963) 1625–1654. doi:10.1016/0371-1951(63)80161-7.
[53] G.A. Wheaton, L.J. Stoel, N.B. Stevens, C.W. Frank, Optical Spectra of Phenazine, 5,10-Dihydrophenazine, and the Phenazhydrins, Appl. Spect. 24 (1970) 339–343. doi:10.1366/000370270774371642.
[54] R.E. Hester, K.P.J. Williams, Free radical studies by resonance Raman spectroscopy. The 5,10-dihydrophenazine and 5-methyl-10-hydrophenazine radical cations, J. Raman Spectr. 13 (1982) 91–95. doi:10.1002/jrs.1250130115.
[55] W.-H. Li, X.-Y. Li, N.-T. Yu, Surface-enhanced hyper-Raman scattering and surface-enhanced Raman scattering studies of electroreduction of phenazine on silver electrode, Chem. Phys. Lett. 327 (2000) 153–161. doi:10.1016/S0009-2614(00)00852-6.
[56] R.H. Sestrem, D.C. Ferreira, R. Landers, M.L.A. Temperini, G.M. do Nascimento, Synthesis and spectroscopic characterization of polymer and oligomers of ortho-phenylenediamine, Eur. Polym. J. 46 (2010) 484–493. doi:10.1016/j.eurpolymj.2009.12.007.
[57] I.H. Wasbotten, T. Wondimagegn, A. Ghosh, Electronic Absorption, Resonance Raman, and Electrochemical Studies of Planar and Saddled Copper(III) meso-Triarylcorroles. Highly Substituent-Sensitive Soret Bands as a Distinctive Feature of High-Valent Transition Metal Corroles, J. Am. Chem. Soc. 124 (2002) 8104–8116. doi:10.1021/ja0113697.
[58] A.A. Hermas, M. Nakayama, K. Ogura, Enrichment of chromium-content in passive layers on stainless steel coated with polyaniline, Electrochim. Acta. 50 (2005) 2001–2007. doi:10.1016/j.electacta.2004.09.008.

[59] R. Yamuna, S. Ramakrishnan, K. Dhara, R. Devi, N.K. Kothurkar, E. Kirubha, et al., Synthesis, characterization, and nonlinear optical properties of graphene oxide functionalized with tetra-amino porphyrin, J Nanopart Res. 15 (2013) 1–9. doi:10.1007/s11051-012-1399-y.
[60] R. Zanoni, T. Boschi, S. Licoccia, R. Paolesse, P. Tagliatesta, An XPS study of Rh and Co derivatives of tetrapyrrole macrocyles, Inorg. Chim. Acta. 145 (1988) 175–177. doi:10.1016/S0020-1693(00)83952-3.
[61] M. Mateos, R. Meunier-Prest, O. Heintz, F. Herbst, J.-M. Suisse, M. Bouvet, Comprehensive Study of Poly(2,3,5,6-tetrafluoroaniline): From Electrosynthesis to Heterojunctions and Ammonia Sensing, ACS Appl. Mater. Interfaces. 10 (2018) 19974–19986. doi:10.1021/acsami.8b03601.
[62] B. Hirschorn, M.E. Orazem, B. Tribollet, V. Vivier, I. Frateur, M. Musiani, Determination of effective capacitance and film thickness from constant-phase-element parameters, Electrochim. Acta. 55 (2010) 6218–6227. doi:10.1016/j.electacta.2009.10.065.